Biochemical and Biophysical Research Communications 464 (2015) 51–56

Contents lists available at ScienceDirect

Biochemical and Biophysical Research Communications

journal homepage: www.elsevier.com/locate/ybbrc

Non-lethal heat treatment of cells results in reduction of tumor initiation and metastatic potential

Yoo-Shin Kim, Tae Hoon Lee, Brian E. O'Neill*

Department of Translational Imaging, Houston Methodist Research Institute, Weill Medical College of Cornell University, 6670 Bertner Ave., Houston, TX 77030, USA

ARTICLE INFO

Article history:
Received 20 May 2015
Accepted 28 May 2015
Available online 29 May 2015

Keywords:
Hyperthermia
Metastasis
Cancer stem cell
Tumor initiation
Bioluminescence imaging

ABSTRACT

Non-lethal hyperthermia is used clinically as adjuvant treatment to radiation, with mixed results. Denaturation of protein during hyperthermia treatment is expected to synergize with radiation damage to cause cell cycle arrest and apoptosis. Alternatively, hyperthermia is known to cause tissue level changes in blood flow, increasing the oxygenation and radiosensitivity of often hypoxic tumors. In this study, we elucidate a third possibility, that hyperthermia alters cellular adhesion and mechanotransduction, with particular impact on the cancer stem cell population. We demonstrate that cell heating results in a robust but temporary loss of cancer cell aggressiveness and metastatic potential in mouse models. In vitro, this heating results in a temporary loss in cell mobility, adhesion, and proliferation. Our hypothesis is that the loss of cellular adhesion results in suppression of cancer stem cells and loss of tumor virulence and metastatic potential. Our study suggests that the metastatic potential of cancer is particularly reduced by the effects of heat on cellular adhesion and mechanotransduction. If true, this could help explain both the successes and failures of clinical hyperthermia, and suggest ways to target treatments to those who would most benefit.

1. Introduction

Given the complexity of the disease, successful treatment of cancer will ultimately involve taking advantage of synergies between different therapies to overcome the various protective mechanisms supporting tumor growth and metastasis. Hyperthermia, the treatment of tumors with elevated but non-lethal temperature, has long been associated with better treatment outcomes in combination with chemotherapy and radiation therapy in many cases, however, the general response has been highly variable, and not nearly as effective as many would have hoped. If we wish to improve this situation, it is necessary to better understand the effects of hyperthermia at the cellular level. It is well understood generally that heat leads to the denaturation of proteins, the loss of their function, the failure of some cellular pathways and the activation of others [1]. The end result is some probability of cell death that is reasonably characterized by the idea of a "thermal dose", based on the thermal physics controlling denaturation of a generalized protein or set of proteins. The thermal dose is best expressed in terms of an Arrhenius damage model [2–4], or may be approximated in terms of cumulative equivalent minutes at 43 °C [2,5,6]. Several groups are looking at thermal denaturation of individual proteins and families of proteins *in vitro*, and some researchers have attempted used this data to try to predict cellular behavior [4]. Unfortunately, the list of proteins thus analyzed remains short. We feel that it is more pragmatic to track cellular changes due to sub-lethal heat. Knowing these cellular changes may be sufficient for developing therapeutic strategies even before a clear molecular basis for them is established.

One of the critical drivers of this study has been the observation by us and others that there exist differences in susceptibility to heat among cell phenotypes [2,6]. It was suspected some time ago that heat is more lethal to cancerous cells than to normal cells in general, which became the impetus behind much of the hyperthermal therapy applied in the clinic [7,8]. More recently, however, there have been suggestions in the literature that the tumor initiating cell (or cancer stem cell) fraction is more susceptible to heat-plus-radiation than the less virulent non-initiating cancer cells [9,10]. This is important in that it could provide a means of specifically

* Corresponding author. Department of Translational Imaging, Houston Methodist Research Institute, Weill Medical College of Cornell University, 6670 Bertner Ave, R6-123, Houston, TX 77030, USA.
E-mail address: BEOneill@houstonmethodist.org (B.E. O'Neill).

http://dx.doi.org/10.1016/j.bbrc.2015.05.093
0006-291X/

targeting therapy to the most malignant cells in the tumor, the ones that are most capable of evading chemotherapy and establishing metastatic colonies elsewhere in the body. A better understanding of cellular behavior under heat treatment would go a long way towards providing a much needed strategy for targeting hyperthermia where it may be most helpful and away from those who would not benefit from it.

2. Material and methods

In vitro heat shock test on B16F10 melanoma and MDA-MB 231 breast cancer cell line. The mouse melanoma cancer cell line B16F10-Luc and the human breast cancer cell line MDA-MB-231-Luc cells were obtained, tested negative for pathogens and authenticated by Idexx Bioresearch, Inc. (Columbia, MO). B16F10-Luc and MDA-MB-231-Luc cell line were grown in RPMI and DMEM medium respectively (Gibco, Grand Island, NY), containing 1% fetal bovine serum (FBS) and 1% penicillin streptomycin at 37 °C in a humidified atmosphere of 5% CO_2 in air. Cultures were seeded 24 h earlier in a clear-bottom, 96 well black plate with 1% serum medium. Cultures were separated into 2 groups, a sham treated control group (37 °C) and heat shock treated group (43 °C). Each plate was sealed with para-film and put into water bath (37 °C and 43 °C) for 25 min. Cell viability and luciferase activity was measured via MTT assay after heat treatment.

2.1. B16F10 + HT tumor initiation model

All animal procedures were approved by the Institutional Animal Care and Use Committee. Athymic female nude mice (Crl:NU(NCr)-Foxn1nu) (6 weeks old; 20–25 g) were purchased from Charles River. Cells were heat treated as above. Then the mice were prepared with bilateral subcutaneous injections of the hind leg using cell numbers of 1×10^6 and 5×10^6 cells. Tumor cell luminescence was measured by imaging with the Xenogen IVIS-200 at 6, 24 and 72 h post injection. At 12 days post inoculation, the mice were sacrificed and representative organs collected, including tumors, for ex vivo BLI. Tumor dimensions at the final time point were measured using calipers and converted to volumes using the formula for an ellipse.

Viable B16F10-Luc cells in reduced numbers, 5×10^5, 1×10^4, and 1×10^3, were inoculated bilaterally to athymic nude mice as above. The cells on the right were treated at 43 °C for 25 min, and the cells on the left received the sham treatment. Tumor growth was measured every 3 days from the first day post-inoculation to 3 weeks using calipers and BLI. Tumor tissue was collected when the mice were sacrificed on the final day and imaged ex vivo via BLI.

2.2. BLI imaging of mouse melanoma pulmonary metastasis model

Heat treated and sham-treated B16F10-Luc cells were injected into the mouse via tail vein with 100ul complete medium at a dose of 2×10^5 viable cells/mouse. Bioluminescence imaging was used to detect metastatic disease in the lung at 3, 6, 9, 15 and 21 days post injection using Xenogen BLI system. Following sacrifice of the mice, ex-vivo lung tissue was imaged with BLI with metastatic nodules were counted.

2.3. BLI imaging of MDA-MB 231 breast tumor model

Identical viable numbers (5×10^6) of heat and sham-treated MDA-MB 231-Luc cells were administrated to the mammary fat pad of female nu/nu mice. Animals were divided into three groups receiving PBS, sham-treated cells and heat-treated cells. Thirty days after injection, bioluminescence imaging was used to detect primary tumor volume and whole-body metastatic disease. Primary tumor growth was measured until 63 days. The tumor volumes were measured every 3 days and mice imaged weekly to assess metastasis, using the Xenogen IVIS system. At the final time point, the mice were sacrificed to collect tumor tissues and assess metastatic lung tissue using ex vivo BLI.

2.4. Time lapse imaging during heat treatment

Cell culture images were captured over time during and after heating using the ImageXpress Micro High Content Screening System (Molecular Devices, LLC, Sunnyvale, CA). In order to make a reasonable comparison to other *in vitro* and in vivo data, it was necessary to measure temperature in a similar manner and match the thermal dose. Typical treatments were done using the thermal control of a water bath, however, heating under the microscope did not employ a bath, meaning that the timing is somewhat different. An alternative method of measure was introduced, inserting a sub-millimeter thermocouple directly into a well in the plate adjacent to the imaged wells and similarly containing 0.2 ml of fluid. Using this thermocouple, temperature is measured every 5 s and the accumulated thermal dose calculated in near real time on a laptop computer. This system was first deployed during 'standard' heat treatment to establish the thermal dose associated with the bath, then during heat treatment under the microscope to obtain a similar dose while imaging. The temperature controller for the ImageXpress chamber was altered to ensure that we could reach 43 °C in the plate within a reasonable time. The work flow was as follows. First, the chamber was heated to 37–38 °C. Then, the plate was introduced and imaging began. The chamber was heated while measuring thermal dose, typically reaching a peak temperature around 43 °C after 10 min or so. When the sample was a few minutes away from the target thermal dose, the plate was cooled as rapidly as possible, by opening the chamber to room temperature air. Due to the need to rapidly reduce the temperature in this way, images could not be captured during the cool-down, which could also take several minutes. Once cooled to 37 °C, the chamber was once again closed and imaging began again, concluding approximately 6 h after heating started. Each plate had 9 wells containing cells, and brightfield and fluorescent images were captured at 4 locations within each well prior to moving to the next well. During the first imaging cycle, the system was set to automatically adjust the focus relative to the bottom of the plate, while the remaining images were taken using the focus established during the first round. Excluding the first round, the system was successful in capturing a complete set of images every 5 min. The entire sequence was stored for offline analysis.

2.5. Image analysis and statistics

Images captured during and following heating were used to assess a number of parameters in heated and unheated cells. First, the cell proliferation was directly assessed by quantifying fission events during mitosis; second, gross changes in cell morphology were quantified. Finally, changes in mobility were found by tracking cell movement over time.

Quantification of both cell proliferation and morphology were done by "hand counting" assisted by ImageJ software (v.1.48u, National Institutes of Health, USA). The reason for this approach was that a number of the wells were highly confluent, making automatic cell recognition in the brightfield images error prone and unreliable. Five image locations in different wells were randomly selected for the quantification and used for both the cell proliferation and morphology analysis. At each location, a box was drawn in ImageJ to include the same set of arbitrarily chosen 70-

150 cells in each image in the series. Great care was taken to ensure that the boxes drawn were in the same physical location based on visual correlation of cells and non-cellular artifacts. Although the ImageXpress system demonstrated great reliability in returning to locations within sequences, opening and closing the plate cover to cool the cells typically resulted in translations of hundreds of microns to a millimeter. Within the boxes, the mostly spherical "rounded" or "balled" cells were counted, along with the total number of cells both prior to heating and again at the 5 h timepoint. The change in the percentage of balled cells was determined and compared between groups. The same boxes were used to count cellular fission events through the first 2.5 h. The percentage of cells undergoing fission/hour was calculated and compared between the heat treated groups and control. Differences between groups were tested using one-way ANOVA and Tukey HSD in R [11].

Cell mobility in the hours following treatment was assessed in the following manner. Images from a selected well and location were opened as a "stack" in ImageJ. A box was drawn containing 50–70 cells whose motion was to be quantified. As well, one or more visible defects or droplets, presumed to move with the plate, were chosen. The locations of each cell in the box as well as the defects were tracked at each time using MTrackJ [12], an ImageJ plugin designed to assist in that purpose. The results were recorded and loaded into a spreadsheet for manipulation, and finally into R for statistical analysis. The speed of the cells between each time interval was calculated from the data as the change in cell location minus the change in defect (plate) location divided by the time increment. The resulting speeds were plotted on a histogram in R at different times. A linear mixed effects model (package *lme4* [13]) was used to analyze the changes in speed over time for the different heat treatments, with a random term (TID = track ID) to correct for repeated measures of the same cells over time.

3. Results

3.1. Effect of heating on tumor initiation in vivo

In the B16F10-Luc mouse melanoma tumor xenograft model, tumor growth and virulence were significantly retarded by heat treatment. In preliminary studies using a single mouse, the sham treated tumor volume (inoculated with 37 °C sham treated control cells) grew much faster than the HT treated tumor volume (inoculated with 43 °C HT cells), as measured with calipers. Bioluminescence activity was observed on both sides starting at 6 h post inoculation. At 24 and 72 h post inoculation, the BLI signal was markedly different. The same pattern was found with using different cell numbers (1×10^6 and 5×10^6 cells inoculated). The final tumor volume at 12 days post-inoculation was found to be much greater in the sham treated controls than in the HT tumors (6-fold and 4-fold larger respectively for 1×10^6 and 5×10^6 cells) (**Sup. 3**). The effect of heat treatment in blocking tumor initiation was studied with B16F10-Luc. As shown in Fig. 1, heat treated cells showed significant loss of tumor initiation and growth compared to sham treated controls. Mice injected with heat treated B16F10-Luc cells (5×10^5 cells) had 4 fold lower tumor volume than the sham treated control group by the end point of day 21. From day 9, the control tumor slowly increased in volume and then rapidly grew after day 12. On the other hand, the heat treated group was barely palpable beginning at day 12 and slowly grew until end point at day

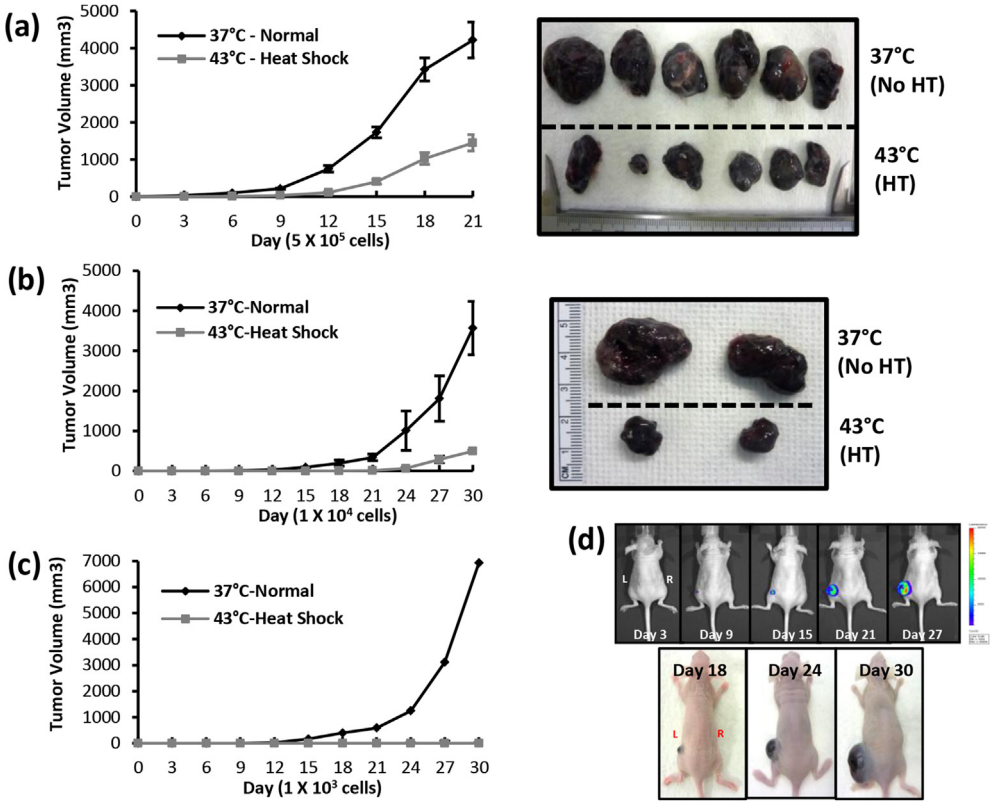

Fig. 1. Effect of heating on tumor initiation and growth. Three different viable cell numbers 5×10^5, 1×10^4 and 1×10^3 of B16F10-Luc cancer cells were used to inoculate nude mice on either leg (left: sham treatment, right: heat treatment) and tumor growth was measured every 3 days **(4a, b, c)**. Tumor tissue was collected when the mice were sacrificed at day 30. The results demonstrate effect of heat treatment on the tumor initiating cell fraction (TIC). Below 1000 cells, heat treated cells fail to form a tumor while sham treated cells grow normally.

21 (Fig. 1a). Reducing the cell number from 5×10^5 to 1×10^4 (50 fold) produced a stronger effect with a 10 fold to drop in tumor volume of the HT group compared to the control group at 30 days (Fig. 1b). A further drop in cell number from 1×10^4 to 1×10^3 (10 fold) resulted in a complete block of the tumor growth in heat treated group. At the end point of day 30, the tumor volume of sham treated control group was over 7000 mm^3, in contrast, tumor volume of HT group was at or close to zero (<10 mm^3) (Fig. 1c). Bioluminescence imaging (BLI) was unable to detect a signal from the heat treated cells on days 3, 9, 15, 21, 27. (Fig. 1d).

3.2. Loss of metastatic potential due to heat shock on pulmonary metastasis mouse

The pulmonary metastasis model is widely used for the evaluation of anti-metastatic therapy in many tumor models, including B16 melanoma. In this model, the sham treated (at 37 °C) control group showed a faintly observed metastatic signal from the lungs 3 days following tail vein injection of 2×10^5 B16F10-Luc, and a clearly observed signal at 7 days. In contrast, the HT group (at 43 °C) had no signal at either time point (Fig. 2a). With higher cell numbers (5×10^5), the luminescence signal rapidly increased from day 6 to day 21. On the other hand, the HT group still had no signal even at 21 days (Fig. 2b). The mice were sacrificed at day 21 and the lung tissue collected for ex vivo bioluminescence imaging and visual inspection. The lung tissue of the sham treated group had numerous black nodules. However, in the HT group, few lung nodules were visible. Comparing nodule numbers between sham treated and HT group showed significant differences (Fig. 2c).

3.3. Heat shock inhibits metastasis and slows primary tumor growth in an orthotopic breast cancer model

We performed in vivo metastasis and long term recurrence experiments using HT and sham treated MDA-MB 231 expressing luciferase. As shown in Fig. 3a, primary tumor growth and metastatic invasion was inhibited by HT compared to the sham treated control group for the initial 30 days. In Fig. 3b, the primary tumor volume was significantly greater in the sham treated control than the HT group beyond 60 days. At the final time point, the mean primary tumor size in the HT group was about 5 times smaller than in the sham control group (Fig. 3c). *Ex vivo*, lung tissue from the sham treated control group had highly expressed luminescence signal but the HT group had a very weak signal (Fig. 3d). All other organs including liver, spleen, kidney, and heart had almost no or minimal signal compared to the lung (data not shown).

3.4. The effect of heat treatment on cell mobility, proliferation and shape

The thermal dose for HT MDA-MB-231 cells treated in bath for 30 min was measured to be equivalent to 40 ± 3 CEM43 (Cumulative Equivalent Minutes at 43 °C). Cells treated with heat under the microscope receiving 42 CEM43 thermal dose (HT) demonstrated significant changes in both morphology and mobility compared to cells receiving either 0 or 23 CEM43 (Fig. 4a). The shape of the 23 CEM43 was not significantly different and from that of the unheated cells. However, cells receiving 42 CEM43 showed significant ($p < 0.0009$) 24 ± 6% increase in rounding or balling over the ensuing several hours (Fig. 4b). This was obviously greater than the change in balled cell number found for both the 0 and 23 CEM treated cells. Both the HT cells and the 23 CEM43 cells showed an almost total loss of mitotic activity (Fig. 4c) in the 5 h following treatment when compared to untreated cells, dropping from 2.3 ± 0.7% of control cells undergoing mitotic fission each hour to 0.1 ± 0.2% per hour for the 23 CEM43, and down to total mitotic arrest for the 42 CEM43 HT cells over 5 h.

The HT cells also showed a significant ~50% drop in mobility over time compared to no change for the control cells (Fig. 4f vs. Fig 4d), from 0.45 μm/min down to 0.16 μm/min. The linear mixed effects model controlling for repeated measures of each cell gave a highly significant ($p < 0.0001$) deceleration of 0.0012 μm/min2. The 23

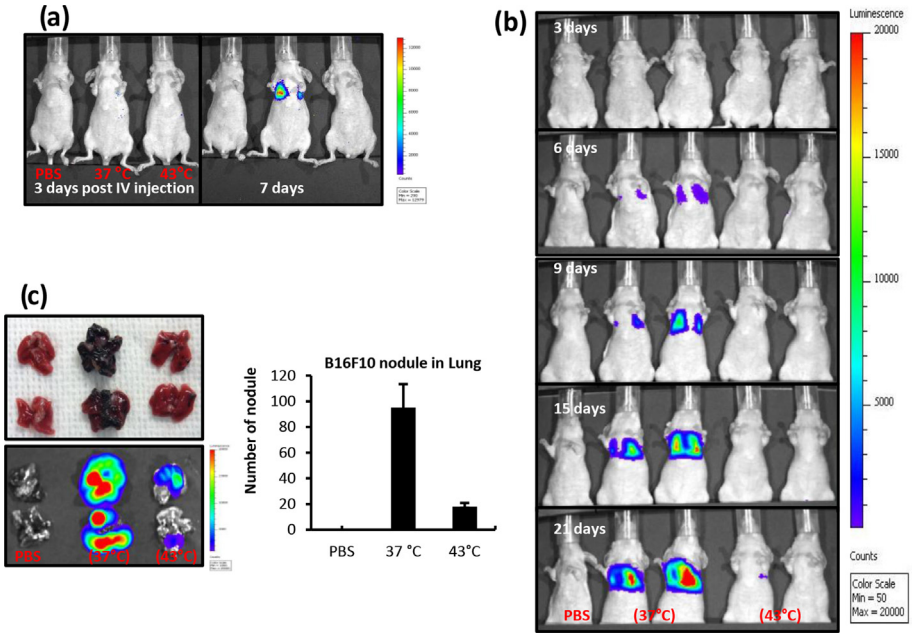

Fig. 2. BLI imaging of mouse melanoma pulmonary metastasis model. Identical numbers (2×10^5) of viable heat treated and sham treated B16F10-Luc cells were injected into the mouse via tail vein. Bioluminescence imaging (BLI) used to detect metastatic disease in the lung at 3 and 7 days post injection failed to find metastatic disease from the heat treated cells **(5a)**. The study was repeated using a higher number (5×10^5) of cells, with imaging at 3, 6, 9, 15, 21 days **(5b)**. The lung was extracted when the mice were sacrificed on day 21, imaged ex vivo with BLI and nodules counted **(5c)**. These results demonstrate a significant reduction in metastatic potential of the heat treated cells.

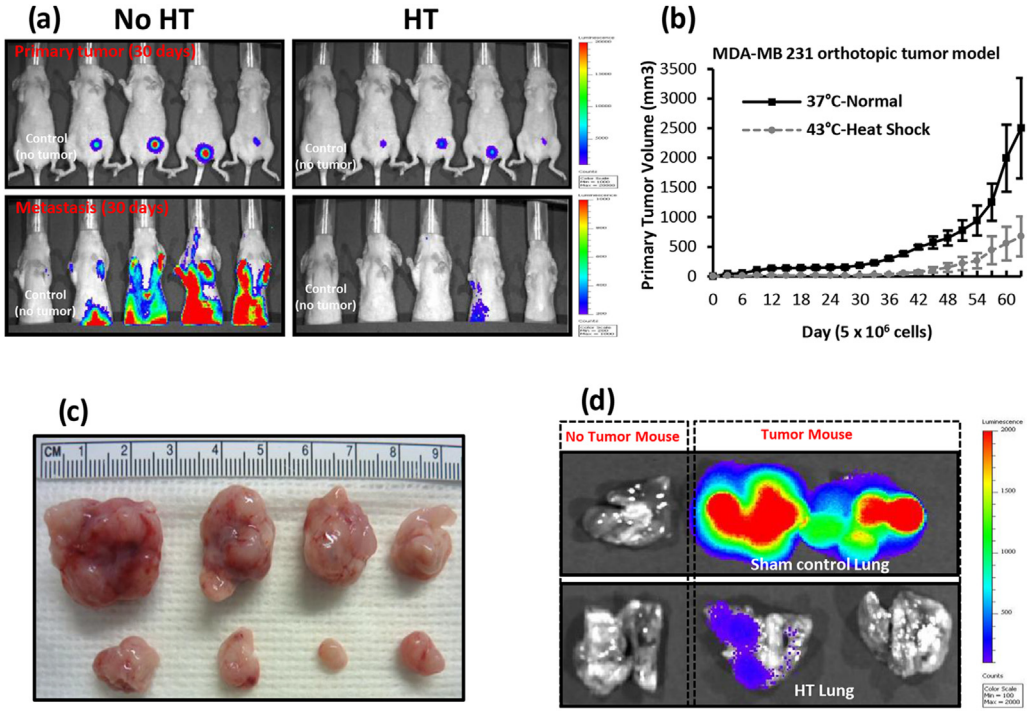

Fig. 3. BLI imaging of MDA-MB 231-Luc metastatic breast tumor model. 5×10^6 viable heat and sham treated MDA-MB 231-Luc cells were administered orthotopically to the mammary fat pad of nude mice. Thirty days post inoculation, bioluminescence imaging was used to detect primary tumor **(6a, upper)** and metastatic events in the whole body **(6a, bottom)**. **(6b)** indicates primary tumor growth out to 63 days, when the mice were sacrificed for collection of tumor **(6c)** and lung **(6d)** tissues. Heat treatment results in a reduction of both primary tumor growth and metastatic growth in this tumor model.

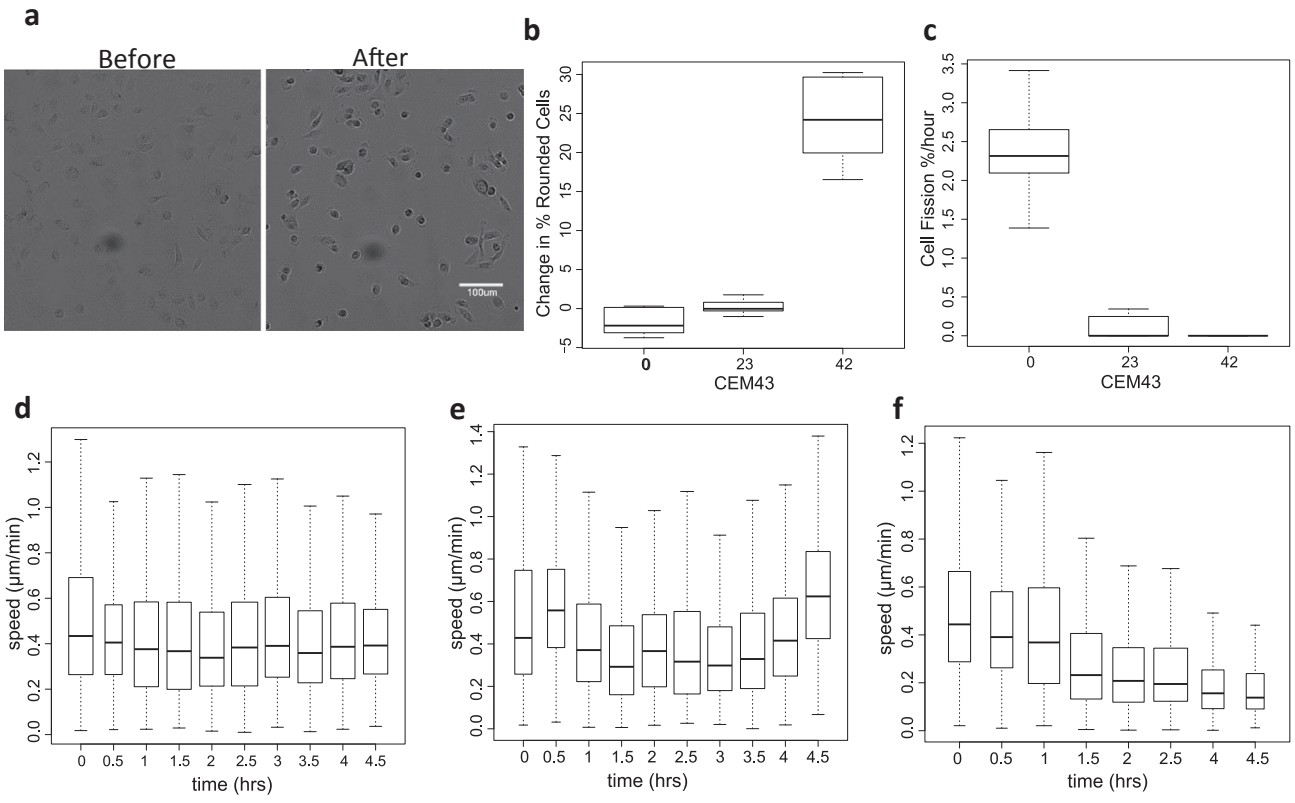

Fig. 4. Changes in cell behavior with heating. MDA-MB-231 breast cancer cells were imaged under time lapse microscopy during and following heating at 3 different thermal doses. **(4a)** Morphology change are clearly visible in heat treated (42 CEM43) cells, with observable "rounding" or "balling" that last up to 5 h after treatment. This morphological change did not happen at the lower thermal doses **(4b)**. Heated cells undergo a drastic reduction in mitotic fission events, even at the lower thermal dose of 23 CEM43 **(4c)**. Both of these changes are reversed within a day or two (data not shown). **Cell speed as a function of time for heat treated cells**. MDA-MB-231 cells were tracked over time during and after heat treatment (heat applied at time 0). At a thermal dose of 0 CEM43 **(4d)**, cell motion continues unabated. At the maximum HT thermal dose of 42 CEM43 **(4e)**, cell motion is halved over the ~5 h following heat treatment. For the 23 CEM43 thermal dose **(4f)**, the motion initially slows but recovers by the end of 5 h.

CEM43 cells' mobility also initially dropped but recovered by the end of 5 h (Fig. 4e).

4. Discussion

Thermal treatment of cells is known to result in protein denaturation, however, which proteins are denatured at what temperature or thermal dose is still largely a matter of speculation. Our results tend to suggest that some of the earliest targets of heat treatment lie in those proteins that are related to cell adhesion, cell shape, and cell mobility. These proteins could be integrins, tubulins, actin, or many others. This is in line with observations in other tissues, where hyperthermia and thermal injury is known to result in a nearly instantaneous drop in interstitial pressure that is best explained by a loss of cellular adhesion [14,15]. Whatever the case may be, the clear result in cancer cells appears to be a robust loss of tumorgenicity and tumor aggressiveness, even without loss of tumor viability. One possible explanation for this effect might be that the tumor initiating cells or cancer stem cells are more sensitive to the loss of these proteins then the bulk of cancer cells. There is evidence that at least some tumor-initiating cells or cancer stem cells are highly sensitive to their microenvironment [16–19]. This would suggest that they are also highly dependent on the proteins that allow them to sense and interact with this microenvironment. Such a scenario could explain local/regional hyperthermia's limited clinical value, in that it will have no effect on the already circulating tumor cells. However, it also points to a strategy for leveraging metastatic cells' sensitivity to heat to improve cancer survival by reducing metastatic potential prior to surgery or ablation. Further study would be required to validate this mechanism and to establish appropriate protocols to optimize treatment timing.

Conflicts of interest

The authors disclose no potential conflicts of interest.

Acknowledgments

Time Lapse Imaging services were performed at the HMRI Advanced Cellular and Tissue Microscope (ACTM) Core Facility and bioluminescent imaging was done in the HMRI Preclinical Imaging Core facilities. The authors thank Dr. Dong-soon Choi, for technical support and comments (Houston Methodist Research Institute). This study was partially funded by NIH grant R01 EB009009.

Appendix A. Supplementary data

Supplementary data related to this article can be found at http://dx.doi.org/10.1016/j.bbrc.2015.05.093.

Transparency document

Transparency document related to this article can be found online at http://dx.doi.org/10.1016/j.bbrc.2015.05.093.

References

[1] A. Bettaieb, P.K. Wrzal, D.A. Averill-Bates, Hyperthermia: cancer treatment and beyond, in: L. Rangel (Ed.), Cancer Treatment – Conventional and Innovative Approaches, InTech, 2013.
[2] M.W. Dewhirst, B.L. Viglianti, M. Lora-Michiels, M. Hanson, P.J. Hoopes, Basic principles of thermal dosimetry and thermal thresholds for tissue damage from hyperthermia, Int. J. Hyperth. 19 (2003) 267–294.
[3] K.R. Diller, Stress protein expression kinetics, Annu Rev. Biomed. Eng. 8 (2006) 403–424.
[4] F. Despa, D.P. Orgill, J. Neuwalder, R.C. Lee, The relative thermal stability of tissue macromolecules and cellular structure in burn injury, Burns 31 (2005) 568–577.
[5] S.A. Sapareto, W.C. Dewey, Thermal dose determination in cancer therapy, Int. J. Radiat. Oncol. Biol. Phys. 10 (1984) 787–800.
[6] P.S. Yarmolenko, E.J. Moon, C. Landon, A. Manzoor, D.W. Hochman, B.L. Viglianti, M.W. Dewhirst, Thresholds for thermal damage to normal tissues: an update, Int. J. Hyperth. 27 (2011) 320–343.
[7] R.A. Vertrees, J.B. Zwischenberger, P.J. Boor, S.D. Pencil, Oncogenic ras results in increased cell kill due to defective thermoprotection in lung cancer cells, Ann. Thorac. Surg. 69 (2000) 1675–1680.
[8] U. Hobohm, Fever therapy revisited, Br. J. Cancer 92 (2005) 421–425.
[9] R.L. Atkinson, M. Zhang, P. Diagaradjane, S. Peddibhotla, A. Contreras, S.G. Hilsenbeck, W.A. Woodward, S. Krishnan, J.C. Chang, J.M. Rosen, Thermal enhancement with optically activated gold nanoshells sensitizes breast cancer stem cells to radiation therapy, Sci. Transl. Med. 2 (2010), 55ra79.
[10] T. Torigoe, Y. Hirohashi, K. Yasuda, N. Sato, Constitutive expression and activation of stress response genes in cancer stem-like cells/tumour initiating cells: potent targets for cancer stem cell therapy, Int. J. Hyperth. 29 (2013) 436–441.
[11] R.D.C. Team, R: a Language and Environment for Statistical Computing, R Foundation for Statistical Computing, Vienna, Austria, 2010.
[12] E. Meijering, O. Dzyubachyk, I. Smal, Methods for cell and particle tracking, Methods Enzym. 504 (2012) 183–200.
[13] D. Bates, M. Maechler, B. Bolker, S. Walker, lme4: Linear Mixed-effects Models Using Eigen and S4, 2014.
[14] H. Wiig, K. Rubin, R.K. Reed, New and active role of the interstitium in control of interstitial fluid pressure: potential therapeutic consequences, Acta Anaesthesiol. Scand. 47 (2003) 111–121.
[15] B.E. O'Neill, H.Q. Vo, H. Shao, C. Karmonik, X. Zhou, K.C. Li, MRI-based prediction of pulsed high-intensity focused ultrasound effect on tissue transport in rabbit muscle, J. Magn. Reson Imaging 38 (2013) 1094–1102.
[16] D.E. Ingber, Cellular mechanotransduction: putting all the pieces together again, FASEB J. 20 (2006) 811–827.
[17] M.J. Bissell, M.A. Labarge, Context, tissue plasticity, and cancer: are tumor stem cells also regulated by the microenvironment? Cancer Cell. 7 (2005) 17–23.
[18] E. Fessler, F.E. Dijkgraaf, E.Melo F. De Sousa, J.P. Medema, Cancer stem cell dynamics in tumor progression and metastasis: is the microenvironment to blame? Cancer Lett. 341 (2013) 97–104.
[19] Y. Feng, J. Wen, P. Mike, D.S. Choi, C. Eshoa, Z.-Z. Shi, Y. Zu, C.-C. Chang, Bone marrow stromal cells from myeloma patients support the growth of myeloma stem cells, Stem Cells Dev. 19 (2010) 1289–1296.